

Models of Procyon A including seismic constraints

P. Eggenberger ^{a,1}, F. Carrier ^a, F. Bouchy ^{a,b}

^a*Observatoire de Genève, 51 Ch. des Maillettes, CH-1290 Sauverny, Suisse*

^b*Laboratoire d'Astrophysique de Marseille, Traverse du Siphon, BP 8, 13376 Marseille Cedex 12, France*

Abstract

Detailed models of Procyon A based on new asteroseismic measurements by Eggenberger et al. (2004b) have been computed using the Geneva evolution code including shellular rotation and atomic diffusion. By combining all non-asteroseismic observables now available for Procyon A with these seismological data, we find that the observed mean large spacing of $55.5 \pm 0.5 \mu\text{Hz}$ favours a mass of $1.497 M_{\odot}$ for Procyon A. We also determine the following global parameters of Procyon A: an age of $t = 1.72 \pm 0.30$ Gyr, an initial helium mass fraction $Y_i = 0.290 \pm 0.010$, a nearly solar initial metallicity $(Z/X)_i = 0.0234 \pm 0.0015$ and a mixing-length parameter $\alpha = 1.75 \pm 0.40$. Moreover, we show that the effects of rotation on the inner structure of the star may be revealed by asteroseismic observations if frequencies can be determined with a high precision. Existing seismological data of Procyon A are unfortunately not accurate enough to really test these differences in the input physics of our models.

Key words: Stars: individual: Procyon, stars: evolution, stars: oscillations

PACS: 97.10.Cv, 97.10.Sj

1 Introduction

Due to its brightness and proximity, Procyon A constitutes an ideal target to test the input physics of the stellar models and to search for p -mode oscillations.

Hartmann et al. (1975) were the first to calculate stellar models of Procyon A and to compare them to the observational data available at the time. They

¹ E-mail: Patrick.Eggenberger@obs.unige.ch

found a discrepancy between the astrometric mass (Strand 1951) and the lower astrophysical mass deduced from their models. This mass discrepancy was later confirmed by Demarque & Guenther (1988), who also found that overshoot of the convective core had to be included in the models in order to reproduce the observed effective temperature.

To address this problem of mass discrepancy, Irwin et al. (1992) decided to redetermine the astrometric mass of Procyon A. They found a mass in perfect agreement with the previous value of $1.74 M_{\odot}$. Following this redetermination of Procyon’s mass and motivated by several attempts made to detect the signature of oscillation modes, Guenther & Demarque (1993) calculated an array of stellar models for Procyon A including the new OPAL opacities. They concluded that, using OPAL opacities, no convective overshoot was needed to match Procyon’s position in the HR diagram. However, the discrepancy between the astrometric mass and the mass deduced from stellar evolution models still remained.

This discrepancy was solved thanks to new measurements of orbital elements and parallax of the Procyon system by Girard et al. (1996, 2000). They determined an astrometric mass of $1.5 M_{\odot}$ in good agreement with the value supported by stellar models. Using this revised astrometric mass, Chaboyer et al. (1999) calculated a grid of stellar evolution models for Procyon A and investigated their seismic properties. They concluded that the detection of p -modes would serve as a robust test of stellar evolution theory.

The first indication of the presence of p -modes on Procyon A was obtained by Brown et al. (1991), while the first clear detection was made by Martić et al. (1999). By comparing these observations with theoretical predictions and numerical simulations, Barban et al. (1999) confirmed the stellar origin of the observed excess power.

Very recently, individual p -mode frequencies were identified (Eggenberger et al. 2004b, hereafter ECBB04; Martić et al. 2004). However, Matthews et al. (2004) reported that the MOST satellite did not observe any evidence of the expected acoustic oscillations. To explain the apparent discrepancy with previous radial-velocity measurements, Matthews et al. suggested that either both the radial velocity measurements and the MOST observations are dominated by granulation noise, or the properties of the oscillations are different from the theoretical expectations. Christensen-Dalsgaard & Kjeldsen (2004) cast doubt on the fact that granulation dominates the noise, and suspected that the MOST data might be dominated by non-stellar noise. Moreover, new asteroseismic observations with the HARPS spectrograph confirmed the previous Doppler ground-based detections (Bouchy et al. 2004).

In this work, we will combine all non-asteroseismic measurements with aster-

oseismic observations of ECBB04 to investigate which additional constraints are brought by these seismological data. We will thus try to determine a model of Procyon A which best reproduces all these observational constraints using the Geneva evolution code which includes a complete treatment of shellular rotation and atomic diffusion. Moreover, we will investigate the effects of rotation on the global parameters of Procyon A and on the p -mode frequencies.

The observational constraints available for Procyon A are summarized in Sect. 2, while the input physics of the models and the calibration method are described in Sect. 3. The results are presented in Sect. 4 and the conclusion is given in Sect. 5.

2 Observational constraints

2.1 Astrometric data

The astrometric parameters of the visual binary orbit were recently updated by Girard et al. (2000). Using data obtained with the infrared cold coronagraph (CoCo) and with the WFPC2 on board the Hubble Space Telescope, they found a mass of $1.497 \pm 0.037 M_{\odot}$ for Procyon A, with a parallax $\Pi = 283.2 \pm 1.5$ mas. When only the WFPC2 observations are used, a smaller mass is found: $M = 1.465 \pm 0.041 M_{\odot}$. These masses were derived by using the self-consistent parallax of 283.2 ± 1.5 mas. Using the slightly larger parallax measured by Hipparcos ($\Pi = 285.93 \pm 0.88$ mas) with the astrometric parameters of the orbit results in a smaller mass than the one obtained with the parallax of Girard et al. (2000). Indeed, when only the WFPC2 measurements are used, we find a mass of $1.423 \pm 0.040 M_{\odot}$ with the Hipparcos parallax. Thus, we see that the mass of Procyon A lies between 1.42 and $1.5 M_{\odot}$. All of these masses will be considered in our analysis. We will then determine which value is in best accordance with the other observational constraints and in particular with the asteroseismic measurements.

2.2 Effective temperature and chemical composition

For the effective temperature of Procyon A, we adopted $T_{\text{eff}} = 6530 \pm 90$ K (Fuhrmann et al. 1997). Note that the value of 6530 K is also given by Allende Prieto et al. (2002). The chemical composition of Procyon A is nearly solar; we adopted $[\text{Fe}/\text{H}] = -0.05 \pm 0.03$ (Allende Prieto et al. 2002).

2.3 Luminosity

From the compilation of 13 measurements from the literature, Allende Prieto et al. (2002) derived a mean visual magnitude $\langle V \rangle = 0.363 \pm 0.003$ mag for Procyon A. Combining this mean magnitude with the solar absolute bolometric magnitude $M_{\text{bol}, \odot} = 4.746$ (Lejeune et al. 1998) and the bolometric correction from Flower (1996), we find a luminosity $\log L/L_{\odot} = 0.84 \pm 0.02$. Note that this interval in luminosity is compatible with the use of the parallax of Girard et al. (2000) as well as the Hipparcos parallax. Indeed, the changes in L due to the different parallaxes are very small and entirely included in the error bar of 0.02 ($\log L/L_{\odot} = 0.843$ and 0.835 with the parallax of Girard et al. and the Hipparcos parallax respectively).

2.4 Angular diameter

Recently Kervella et al. (2004) measured the angular diameter of Procyon A using the VINCI instrument installed at ESO's VLT Interferometer. They found a limb darkened angular diameter $\theta = 5.448 \pm 0.053$ mas. Using the Hipparcos parallax, they deduced a linear diameter of $2.048 \pm 0.025 D_{\odot}$. The parallax of Girard et al. (2000) gives a linear diameter of $2.067 \pm 0.028 D_{\odot}$.

2.5 Rotational velocity

Allende Prieto et al. (2002) estimated $v \sin i = 3.16 \pm 0.50 \text{ km s}^{-1}$. However, they pointed out that the correct value is probably close to 2.7 km s^{-1} , since the value of 3.16 may be slightly overestimated as a result of the finite numerical resolution of their convection simulation. Thus, we adopted $v \sin i = 2.7 \text{ km s}^{-1}$ with a large error of 1 km s^{-1} in order to encompass the value of $v \sin i = 3.16 \pm 0.50 \text{ km s}^{-1}$. Using $v \sin i = 2.7 \pm 1.0 \text{ km s}^{-1}$ and assuming that the rotation axis of Procyon A is perpendicular to the plane of the visual orbit ($i = 31.1 \pm 0.6^\circ$, Girard et al. 2000), we find a surface rotational velocity of $5.2 \pm 1.9 \text{ km s}^{-1}$ for Procyon A.

2.6 Asteroseismic constraints

Martić et al. (2004) identified individual frequencies in the power spectrum between 300 and 1400 μHz with a mean large spacing of $53.6 \pm 0.5 \mu\text{Hz}$. Using the CORALIE spectrograph, we confirmed the detection of p-modes on Procyon A and identified individual frequencies with a slightly larger mean large

Table 1

Observational constraints for Procyon A. References: (1) Girard et al. (2000), (2) Hipparcos, (3) Allende Prieto et al. (2002), (4) derived from the other observational measurements (see text), (5) Fuhrmann et al. (1997), (6) Kervella et al. (2004), (7) Martić et al. (2004) and (8) Eggenberger et al. (2004b).

		References
Π [mas]	283.2 ± 1.5	(1)
	285.93 ± 0.88	(2)
M/M_{\odot}	1.497 ± 0.037	(1)
	1.465 ± 0.041	(1)
	1.423 ± 0.040	(1)+(2)
V [mag]	0.363 ± 0.003	(3)
$\log L/L_{\odot}$	0.84 ± 0.02	(4)
T_{eff} [K]	6530 ± 90	(5)
$[\text{Fe}/\text{H}]_{\text{s}}$	-0.05 ± 0.03	(3)
θ [mas]	5.448 ± 0.053	(6)
R/R_{\odot}	2.048 ± 0.025	(6)+(2)
	2.067 ± 0.028	(6)+(1)
V_{s} [km s $^{-1}$]	5.2 ± 1.9	(4)
$\Delta\nu_0$ [μHz]	53.6 ± 0.5	(7)
	55.5 ± 0.5	(8)

spacing of $55.5 \pm 0.5 \mu\text{Hz}$ (ECBB04). In this work, we will use the asteroseismic observations of ECBB04 to constrain the models.

All the observational constraints are listed in Table 1.

3 Stellar models

3.1 *Input Physics*

The stellar evolution code used for these computations is the Geneva code including shellular rotation, described several times in the literature (see Meynet & Maeder 2000). We used the new horizontal turbulence prescription of Maeder (2003) and the braking law of Kawaler (1988) in order to reproduce the magnetic braking that undergo the low mass stars when arriving on the main sequence. Two parameters enter this braking law: the saturation velocity Ω_{sat} and the braking constant K . Following Bouvier et al. (1997), Ω_{sat} was fixed to $14 \Omega_{\odot}$ and the braking constant K was calibrated on the sun. We used the OPAL opacities, the NACRE nuclear reaction rates (Angulo et al. 1999) and the standard mixing-length formalism for convection.

In addition to shellular rotation, our models have been computed including atomic diffusion on He, C, N, O, Ne and Mg using the routines developed for the Geneva–Toulouse version of our code (see for example Richard et al. 1996) recently updated by O. Richard (private communication). The diffusion coefficients are computed with the prescription by Paquette et al. (1986). We included the diffusion due to the concentration and thermal gradients, but the radiative acceleration was neglected.

3.2 *Computational method*

The computation of a stellar model for a given star consists in finding the set of stellar modeling parameters which best reproduces all observational data available for this star. For a given stellar mass, the characteristics of a stellar model including the effects of rotation (luminosity, effective temperature, surface metallicity, surface velocity, frequencies of oscillation modes, etc.) depend on five modeling parameters: the age of the star (t hereafter), the mixing-length parameter $\alpha \equiv l/H_p$ for convection, the initial surface velocity V_i and two parameters describing the initial chemical composition of the star. For these two parameters, we chose the initial helium abundance Y_i and the initial ratio between the mass fraction of heavy elements and hydrogen $(Z/X)_i$.

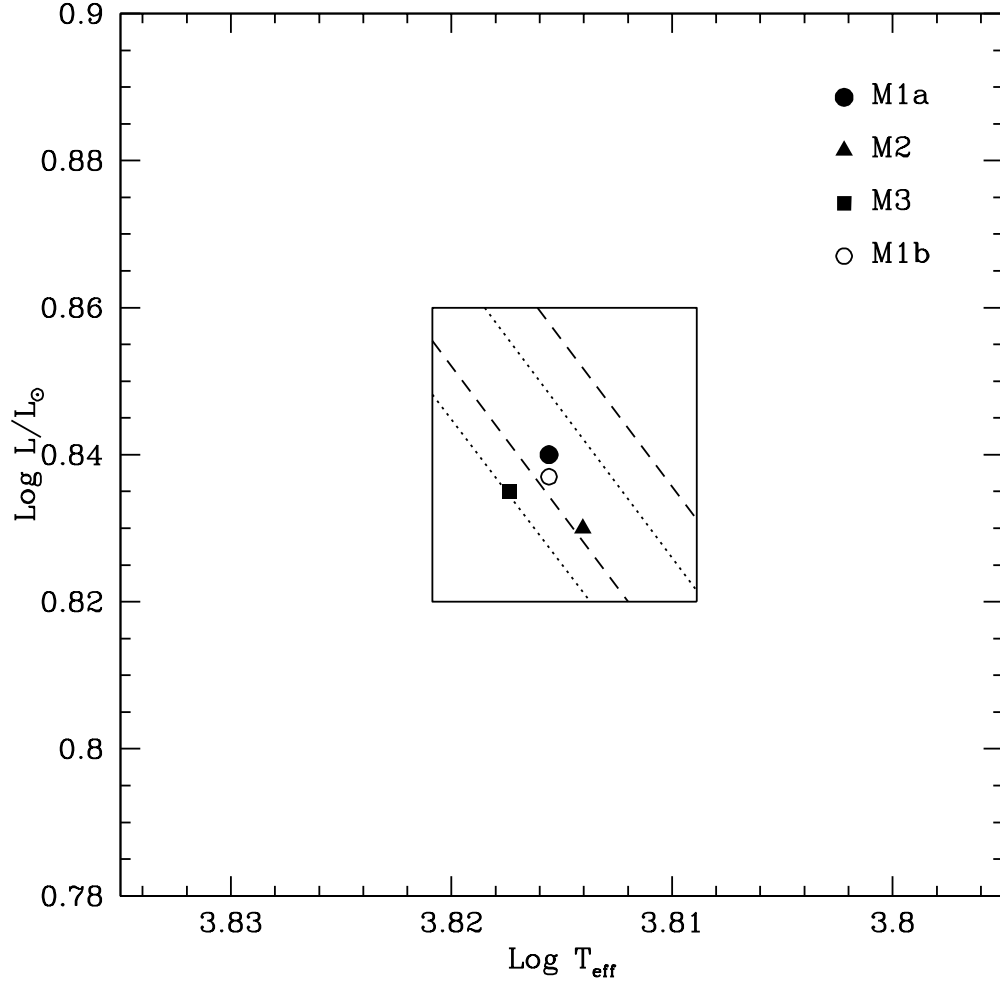


Fig. 1. Observational constraints in the HR diagram for Procyon A. The continuous lines indicate the boxes delimited by the observed luminosity and effective temperature (with their respective 1-sigma errors). The dashed and dotted lines denote the boxes delimited by the interferometric radii deduced using the parallax of Girard et al. (2000) and the Hipparcos parallax, respectively. The positions in the HR diagram of the computed models are indicated (see text and Table 2 for more details).

Assuming that this ratio is proportional to the abundance ratio $[\text{Fe}/\text{H}]$, we can directly relate (Z/X) to $[\text{Fe}/\text{H}]$ by using the solar value $(Z/X)_{\odot} = 0.0230$ given by Grevesse & Sauval (1998). Thus, any characteristic A of a given stellar model has the following formal dependences with respect to modeling parameters : $A = A(t, \alpha, V_i, Y_i, (Z/X)_i)$.

Once fixing the mass of Procyon A to one of the three values listed in Table 1, the determination of the set of modeling parameters $(t, \alpha, V_i, Y_i, (Z/X)_i)$ leading to the best agreement with the observational constraints is made in

two steps. First, we construct a grid of models with position in the HR diagram in agreement with the observational values of the luminosity, effective temperature and radius listed in Table 1. The boxes in the HR diagram for Procyon A corresponding to the three different choices of mass are shown in Fig. 1.

To construct this grid, we proceed in the following way: for a given chemical composition (i.e. a given set Y_i , $(Z/X)_i$) and a given initial velocity V_i , the mixing-length coefficient of each star is adjusted in order to match the observational position in the HR diagram.

Once the position of the star in the HR diagram agrees with the observed values, the surface metallicity of the star is compared to the observed one. If it is out of the metallicity interval listed in Table 1, the models are rejected and the procedure is repeated with another choice of Y_i and $(Z/X)_i$. Note that the surface metallicities $[Fe/H]_s$ are almost identical for the models with the same initial composition and different mixing-length parameters. Moreover, the $[Fe/H]_s$ of the models are mainly sensitive to $(Z/X)_i$ and less to Y_i . As a result, the values of $(Z/X)_i$ are directly constrained by the observed surface metallicity.

Finally, the surface velocity of the models is compared to the observed one; if the velocities of the models are not compatible with the observed value, the models are rejected and the procedure is repeated with another initial velocity (but with the same initial chemical composition). Otherwise, all solutions are kept, since they correspond to models of Procyon A which reproduce all the non-asteroseismic constraints. The whole procedure is then repeated with a new choice of Y_i and $(Z/X)_i$.

In this way we obtain a grid of models with various sets of modeling parameters $(t, \alpha, V_i, Y_i, (Z/X)_i)$ which satisfy all the non-asteroseismic observational constraints of Procyon A, namely the effective temperature, the luminosity, the radius, the surface velocity and the surface metallicity. The second step in determining the best model of Procyon A is to consider the asteroseismic measurements.

For each stellar model of the grid constructed as explained above, low- l p-mode frequencies are calculated using the Aarhus adiabatic pulsation package (Christensen-Dalsgaard 1997). Following our observations, modes of degree $l \leq 2$ with frequencies between 0.6 and 1.4 mHz are computed and the large spacing $\Delta\nu_0$ determined.

Once the asteroseismic characteristics of all relevant models are computed, we perform a χ^2 minimization in order to deduce the set of parameters $(t, \alpha, V_i, Y_i, (Z/X)_i)$ leading to the best agreement with the observations of Procyon A. For this purpose, we define the χ^2 functional

$$\chi^2 \equiv \sum_{i=1}^6 \left(\frac{C_i^{\text{theo}} - C_i^{\text{obs}}}{\sigma C_i^{\text{obs}}} \right)^2, \quad (1)$$

where the vectors \mathbf{C} contains all the observables for the star:

$$\mathbf{C} \equiv (\log L/L_{\odot}, T_{\text{eff}}, R/R_{\odot}, V_s, [\text{Fe}/\text{H}]_s, \Delta\nu_0).$$

The vector \mathbf{C}^{theo} contains the theoretical values of these observables for the model to be tested, while the values of \mathbf{C}^{obs} are those listed in Table 1. The vector $\sigma\mathbf{C}$ contains the errors on these observations which are also given in Table 1.

4 Results

4.1 Models with a mass of $1.497 M_{\odot}$

We first calculated a grid of models including shellular rotation and atomic diffusion with the mass of $1.497 M_{\odot}$ deduced from data obtained with the infrared cold coronagraph (CoCo) and with the WFPC2 on board the Hubble Space Telescope Girard et al. (2000). This mass has been determined with a parallax of $283.2 \pm 1.5 \text{ mas}$, leading to a radius of $2.067 \pm 0.028 R_{\odot}$ for Procyon A. The models have to match the location of Procyon A in the HR diagram which is given by its radius, luminosity and effective temperature (see Fig. 1).

Once this grid of models was computed, we performed the χ^2 minimization described above. In this way, we found the solution $t = 1.72 \pm 0.30 \text{ Gyr}$, $\alpha = 1.75 \pm 0.40$, $V_i = 14 \pm 8 \text{ km s}^{-1}$, $Y_i = 0.290 \pm 0.010$ and $(Z/X)_i = 0.0234 \pm 0.0015$. The position and the evolutionary track of this model (denoted model M1a in the following) in the HR diagram are shown in Fig. 1 and 5. The characteristics of this model are reported in Table 2. Note that the confidence limits of each modeling parameter given in Table 2 are estimated as the maximum/minimum values which fit the observational constraints when the other calibration parameters are fixed to their medium value.

Concerning the asteroseismic features of this model, the theoretical variation of the large spacings $\Delta\nu_{\ell}$ for $\ell = 0, 1, 2$ with frequency was compared to the observations (Fig. 2). Table 2 and Fig. 2 show that the mean large spacing of the M1a model is in good agreement with the observed value of $55.5 \pm 0.5 \mu\text{Hz}$. Moreover, one can see that the M1a model reproduces the observed variation of $\Delta\nu_{\ell}$ with frequency. However, the dispersion of the observed large spacings

Table 2

Models for Procyon A. The upper part of the table gives the observational constraints used for the calibration. The middle part of the table presents the modeling parameters with their confidence limits, while the bottom part presents the global parameters of the star.

	Models including rotation and atomic diffusion			Model without rotation and diffusion
	M1a	M2	M3	M1b
M/M_{\odot}	1.497	1.465	1.423	1.497
$\log L/L_{\odot}$	0.84 ± 0.02	0.84 ± 0.02	0.84 ± 0.02	0.84 ± 0.02
T_{eff} [K]	6530 ± 90	6530 ± 90	6530 ± 90	6530 ± 90
R/R_{\odot}	2.067 ± 0.028	2.067 ± 0.028	2.048 ± 0.025	2.067 ± 0.028
$[\text{Fe}/\text{H}]_{\text{s}}$	-0.05 ± 0.03	-0.05 ± 0.03	-0.05 ± 0.03	-0.05 ± 0.03
V_{s} [km s^{-1}]	5.2 ± 1.9	5.2 ± 1.9	5.2 ± 1.9	—
$\Delta\nu_0$ [μHz]	55.5 ± 0.5	55.5 ± 0.5	55.5 ± 0.5	55.5 ± 0.5
t [Gyr]	1.72 ± 0.30	1.89 ± 0.30	2.18 ± 0.30	1.77 ± 0.30
α	1.75 ± 0.40	1.90 ± 0.30	1.80 ± 0.30	1.60 ± 0.35
V_{i} [km s^{-1}]	14 ± 8	17 ± 8	17 ± 8	—
Y_{i}	0.290 ± 0.010	0.295 ± 0.015	0.295 ± 0.020	0.280 ± 0.010
$(Z/X)_{\text{i}}$	0.0234 ± 0.0015	0.0229 ± 0.0015	0.0231 ± 0.0015	0.0205 ± 0.0015
$\log L/L_{\odot}$	0.840	0.830	0.835	0.837
T_{eff} [K]	6540	6517	6567	6540
R/R_{\odot}	2.052	2.043	2.024	2.045
V_{s} [km s^{-1}]	5.1	5.1	5.4	—
Y_{s}	0.251	0.262	0.260	0.280
$(Z/X)_{\text{s}}$	0.0204	0.0205	0.0205	0.0205
$[\text{Fe}/\text{H}]_{\text{s}}$	-0.05	-0.05	-0.05	-0.05
$\Delta\nu_0$ [μHz]	55.41	55.59	55.57	55.56

around the theoretical curves is slightly greater than expected taking an uncertainty of $0.57 \mu\text{Hz}$, half of the time resolution, on the frequency determination. The comparison of the theoretical and observed values of the small spacing $\delta\nu_{02} \equiv \nu_{n+1,\ell=0} - \nu_{n,\ell=2}$ between $\ell = 0$ and $\ell = 2$ modes is given in Fig. 6. The mean small spacing of the M1a model and the theoretical variation of this spacing with frequency are compatible with the observed values. However, Fig. 6 clearly shows that the observed small spacings are unfortunately not accurate enough to provide strong constraints to stellar models. This is especially true for the couple of points near 799 and 1136 μHz that are either split by rotation or the secondary peaks are due to noise (see ECBB04). Finally, we compare the theoretical p -mode frequencies of the M1a model to the observed ones by plotting the echelle diagram (Fig. 8). In this figure, the systematic difference $\langle D_\nu \rangle$ (see Sect. 3.2.2 of Eggenberger et al. 2004a) between theoretical and observed frequencies has been taken into account. Indeed, a linear shift of a few μHz between theoretical and observational frequencies is perfectly acceptable, due to the fact that the exact values of the frequencies depend on the details of the star's atmosphere where the pulsation is non-adiabatic.

Model M1a corresponds to the best solution which minimizes the χ^2 functional of Eq. 1. However, the minimization shows that many models with different values of the initial helium abundance and the mixing-length parameter α have a χ^2 only slightly larger than the one of the M1a model, and constitute therefore also good models of Procyon A. This is due to the fact that a decrease/increase of the initial helium abundance Y_i can be compensated by an increase/decrease of the mixing-length parameter α to match the observed position of Procyon A in the HR diagram (see Fig. 3). Thus, we obtain a series of models with approximately the same non-asteroseismic features as those of the M1a model. Moreover, the mean large spacing of these models (which is the only asteroseismic quantity included in our χ^2 functional) is also very close to the value of the M1a model, since it mainly depends on the star's mean density and hence on its radius given that the models have the same mass of $1.497 M_\odot$. This explains why there is a series of models which well reproduced the global stellar parameters considered in our minimization. Amongst these models, the M1a model is in slightly better agreement with these observables. Moreover, when individual theoretical and observational asteroseismic frequencies are compared, one finds that the M1a model is also in slightly better agreement with the asteroseismic observations than the other models (see Fig. 4). However, given the limited accuracy of the observations, and especially of the observed small spacings (which are needed to differentiate models with the same position in the HR diagram but different ages), these differences cannot be considered as really significant.

To investigate the effects of rotation on the structure of the models and therefore on their p -mode frequencies, we decided to redo the entire calibration without including the effects of rotation and atomic diffusion. By perform-

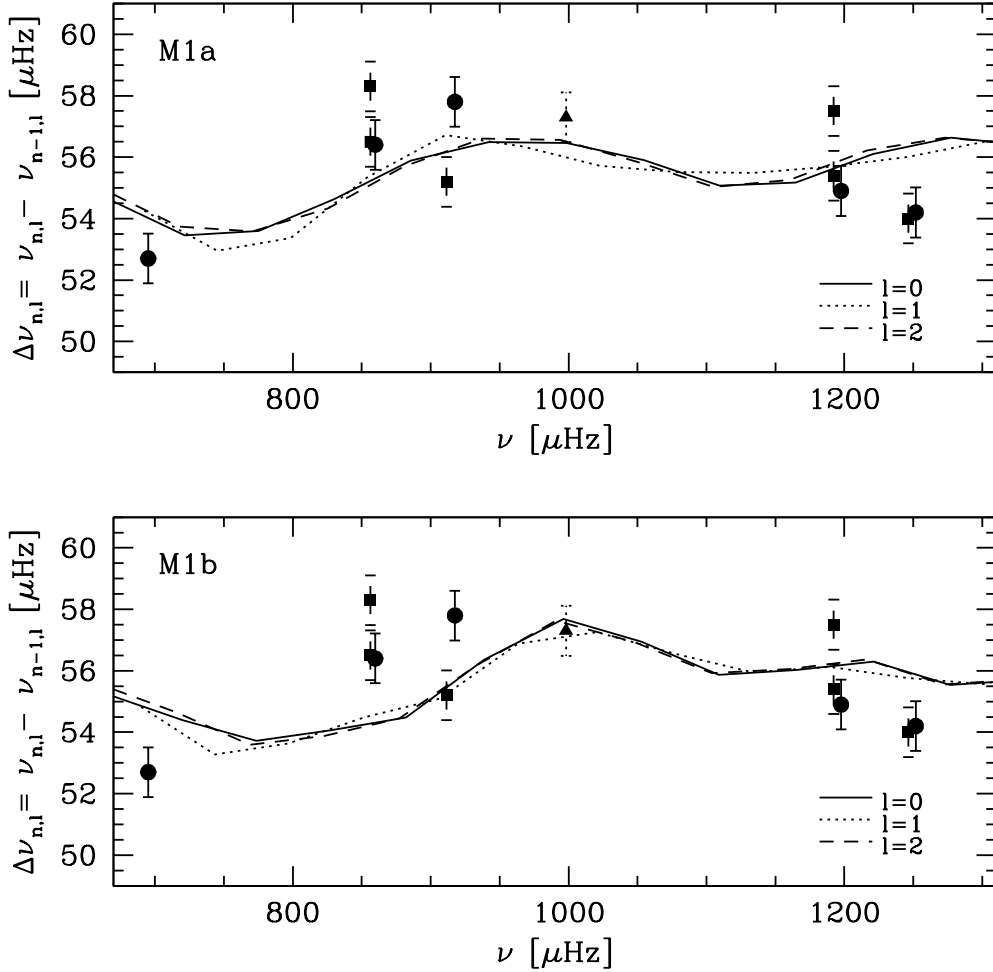


Fig. 2. Large spacing versus frequency for the models with a mass of $1.497 M_{\odot}$. The M1a model includes rotation and atomic diffusion, while the M1b model has been computed without rotation and diffusion (see Table 2). The dots indicate the observed values of the large spacing with an uncertainty on individual frequencies estimated to half the time resolution.

ing the same minimization on this grid of standard models, we found the solution $t = 1.77 \pm 0.30$ Gyr, $\alpha = 1.60 \pm 0.35$, $Y_i = 0.280 \pm 0.010$ and $(Z/X)_i = 0.0205 \pm 0.0015$. The position and the evolutionary track of this model (denoted model M1b in the following) in the HR diagram are shown in Fig. 1 and 5. The characteristics of this model are reported in Table 2. First, we note that the global parameters of this M1b model are very similar to the ones of the M1a model: same effective temperature and approximately same luminosity, radius and mean large spacing as those of the M1a model. Moreover, the ages of both models are very similar. Of course, the initial chemical composition of the models is different, since the M1b model does not take into account the rotationally induced chemical mixing and atomic

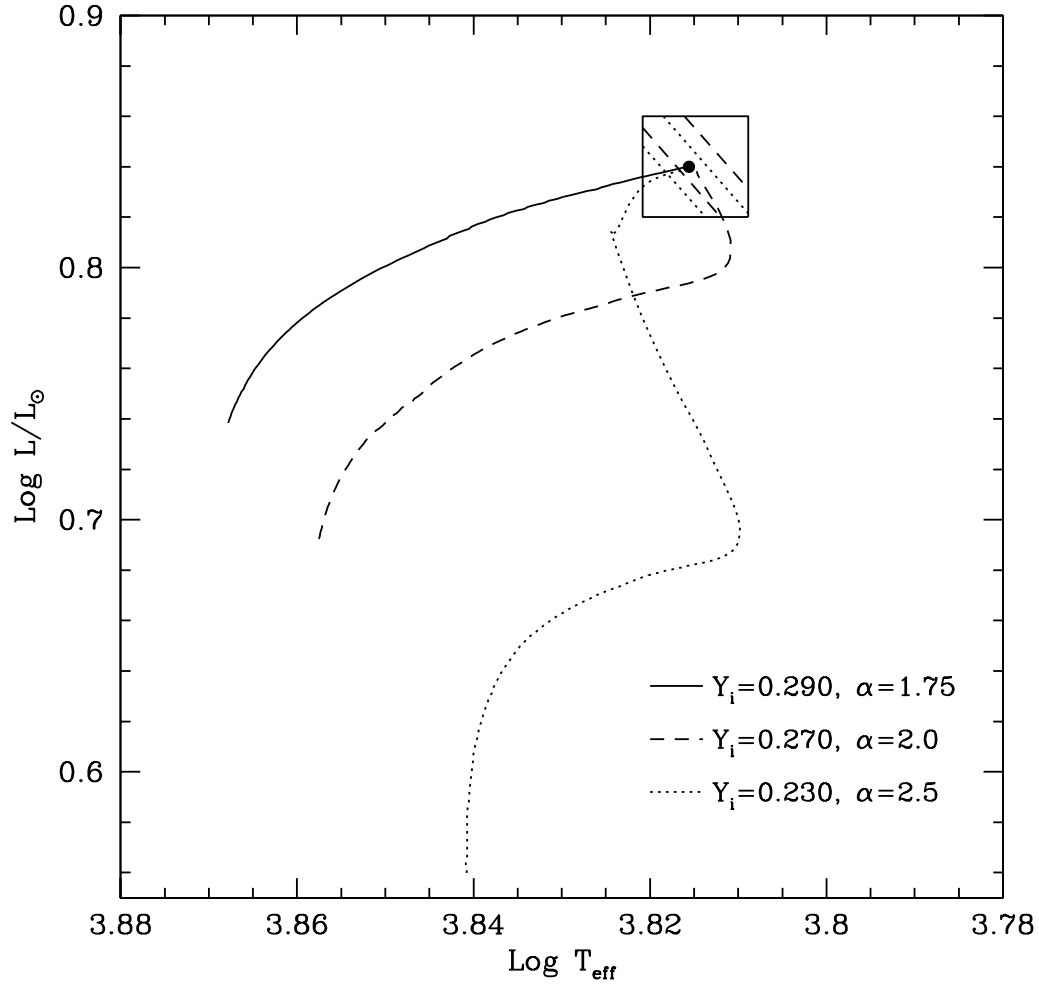


Fig. 3. Evolutionary tracks in the HR diagram for three models of $1.497 M_{\odot}$ with different values of the initial helium abundance Y_i and the convection parameter α . All models include atomic diffusion and rotation. This shows that a decrease in the initial helium abundance Y_i can be compensated by an increase of the convection parameter α in order to reach the same location in the HR diagram.

diffusion. Moreover, the mixing-length parameter of both models is approximately equal to the solar calibrated value determined by using the same input physics ($\alpha_{\odot} = 1.75$ with rotation and atomic diffusion, and $\alpha_{\odot} = 1.59$ without rotation and diffusion).

Concerning the asteroseismic features of the M1b model, the comparison between observed and theoretical variation of the large spacings $\Delta\nu_{\ell}$ is shown on Fig. 2. This figure and Table 2 show that the mean large spacing and the variation of the large spacings with frequency of the M1b model are in good agreement with the observations. Thus, one can see that there are no significant differences between the large spacings of both M1 models; the mean

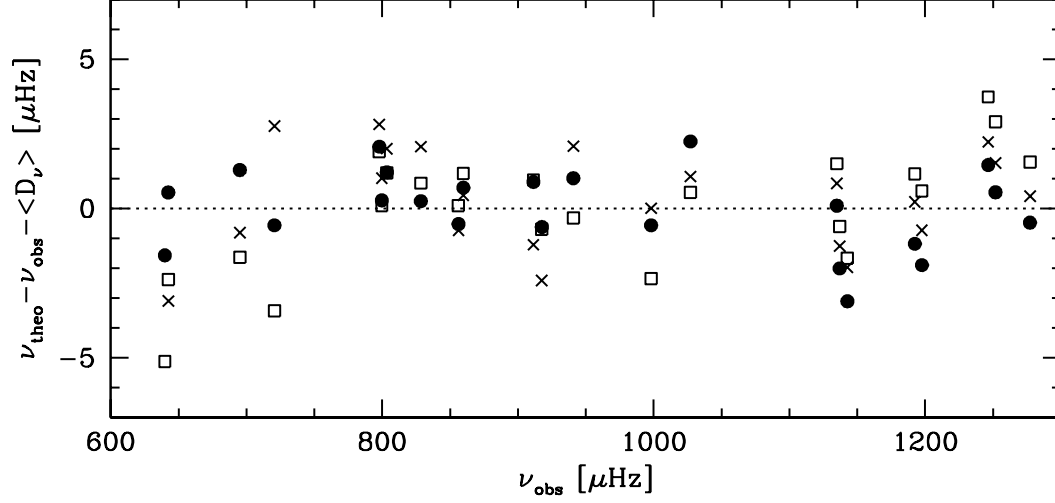


Fig. 4. Differences between calculated and observed frequencies for the models with $1.497 M_\odot$ including rotation and atomic diffusion with different values of the initial helium abundance Y_i and the convection parameter α . Filled circles correspond to the model with $Y_i = 0.290$ and $\alpha = 1.75$ (model M1a), while open squares and crosses designate models with $Y_i = 0.270$, $\alpha = 2.0$ and $Y_i = 0.230$, $\alpha = 2.5$, respectively. The systematic shifts $\langle D_\nu \rangle$ have been taken into account (see text for more details).

large spacing of the M1b model is only slightly larger than the one of the M1a model, which results from the smaller radius of this model compared to the one of the M1a model.

To investigate the effects of rotation on the p -mode frequencies, it is much more interesting to consider the small spacings $\delta\nu_{02} \equiv \nu_{n+1,\ell=0} - \nu_{n,\ell=2}$ which are mainly sensitive to the stellar core. Indeed, as already pointed out by Di Mauro & Christensen-Dalsgaard (2001) and Provost et al. (2002), these spacings may enable a test for overshoot if sufficiently precise frequencies could be determined. To check this, we also computed a model of Procyon A without rotation and atomic diffusion, but with an overshoot of the convective core into the radiative zone on a distance $d_{\text{ov}} \equiv \alpha_{\text{ov}} \min[H_p, r_{\text{core}}]$. Following Schaller et al. (1992), we fixed the value of α_{ov} to 0.2, which is the amount of overshooting usually chosen for non-rotating stellar models. The evolutionary track of this model is shown on Fig. 5. We find that the values of the small spacings of stellar models including overshooting are slightly smaller than those computed for models without overshooting. This can be seen in Fig. 6, where the small spacings of two non-rotating models (one with and the other without overshooting) with the same averaged large spacing are compared. In the same way, it is interesting to note that these differences also exist between the non-rotating model without overshooting (model M1b) and the M1a model calculated with rotation and atomic diffusion, but without overshooting. Indeed, Fig. 6 shows that the non-rotating model (M1b) exhibits slightly higher values of the small spacings than the rotating one (M1a). Thus, we see that

p -mode frequencies indicate that the inclusion of rotation mimics an increase of the overshoot parameter. This results from the fact that, for sufficiently low initial velocities ($v_{\text{ini}} \lesssim 300 \text{ km s}^{-1}$) rotation acts as an overshoot, extending the main sequence tracks towards lower effective temperatures (see Fig. 5).

Even if these theoretical considerations are interesting to point out, it is evidently not necessary to say that, from an observational point of view, we are very far from the precision required to discuss these subtle differences. As mentioned above, we can only conclude that the observed frequency differences between $\ell = 0$ and $\ell = 2$ modes are compatible with theoretical expectations, but are not accurate enough to enable us to test the input physics of our stellar models.

4.2 Models with a mass of $1.465 M_{\odot}$

After having calculated stellar models with the mass of $1.497 M_{\odot}$ determined by Girard et al. (2000), we computed a grid of models with a mass of $1.465 M_{\odot}$. This mass was deduced using only the WFPC2 measurements with the parallax of Girard et al. (2000). Accordingly, the value of the observed linear radius remains unchanged ($2.067 \pm 0.028 R_{\odot}$). All models include shellular rotation and atomic diffusion.

Using this new value for the mass, we found the following solution: $t = 1.89 \pm 0.30 \text{ Gyr}$, $\alpha = 1.90 \pm 0.30$, $V_i = 17 \pm 8 \text{ km s}^{-1}$, $Y_i = 0.295 \pm 0.015$ and $(Z/X)_i = 0.0229 \pm 0.0015$. The position of this model (denoted model M2 hereafter) in the HR diagram is shown in Fig. 1, while its characteristics are given in Table 2.

We note that the modeling parameters of this M2 model are very similar to the ones of the M1a model. Indeed, the initial chemical composition of both models are approximately identical, with a nearly solar initial metallicity which decreases during the star evolution to reach the observed value of $[\text{Fe}/\text{H}]_s = -0.05$. The mixing-length parameter and the initial velocity are only slightly larger for the M2 model than for the M1a. Due to the lower mass, the age of the M2 model is somewhat larger than the one of the M1 models. Note that the large error of 8 km s^{-1} on the initial velocity is due to the large error on the observed surface rotational velocity (relative error of about 35 %), while the large error on the mixing-length parameter α simply reflects the fact that the models are not very sensitive to a change of this parameter.

Using this lower mass leads to a model whose global parameters still reproduce the observational constraints. However, the agreement between observed and theoretical non-asteroseismic parameters is slightly better for the more massive M1 models, than for this model. Concerning the asteroseismic features, one can see that the observed large spacings are well reproduced by the

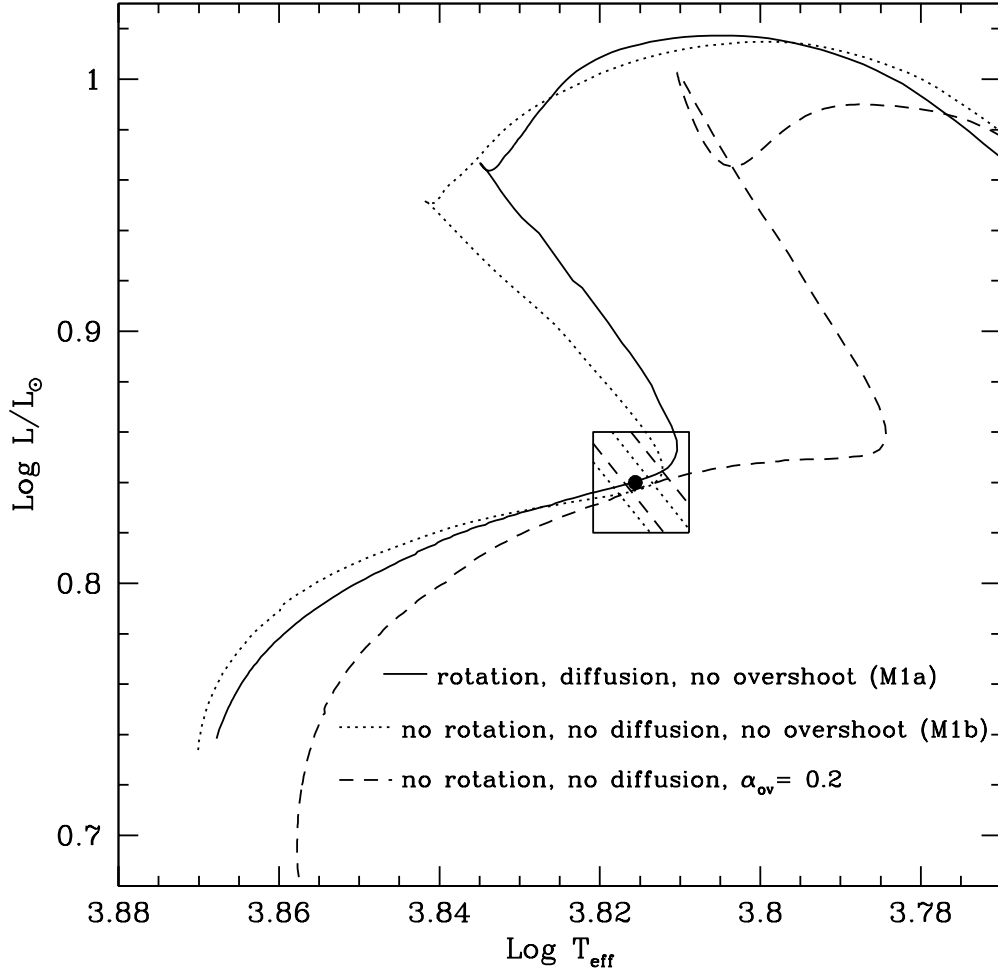


Fig. 5. Evolutionary tracks in the HR diagram for three models of $1.497 M_{\odot}$. The continuous line corresponds to the model including rotation and atomic diffusion but no overshooting (model M1a). The dotted line denotes the model without rotation, atomic diffusion nor overshooting (model M1b), while the dashed line corresponds to a model computed with overshooting ($\alpha_{ov} = 0.2$), but without rotation and atomic diffusion. The dot shows the location of the M1a model.

M2 model (see Fig. 7). Finally, the echelle diagram of Fig. 8 shows that the theoretical frequencies of the M2 model are compatible with the asteroseismic observations, even if the agreement is slightly better for the more massive M1 models than for this model. However, the limited accuracy of the seismological measurements (especially for the observed small spacings $\delta\nu_{02}$) does not enable us to formally reject the M2 model.

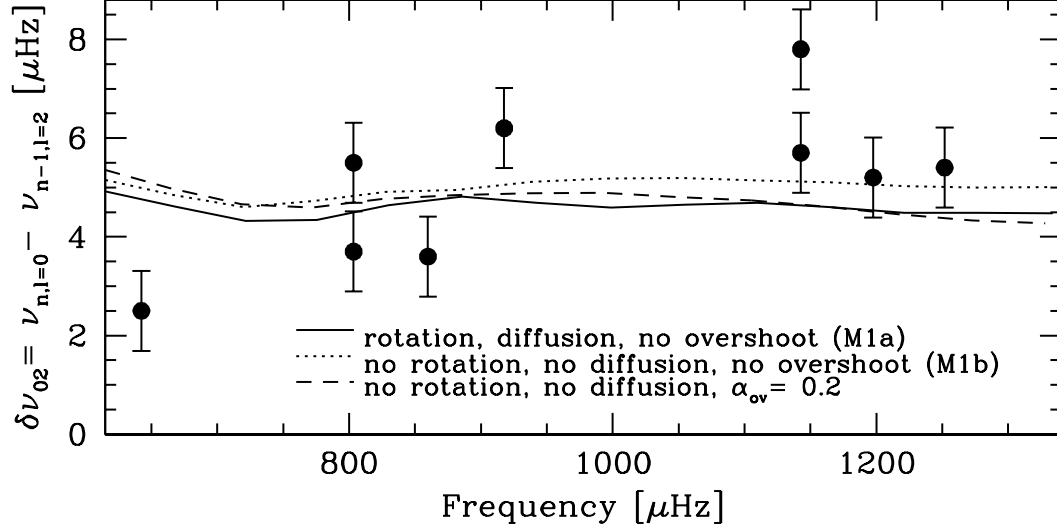


Fig. 6. Small spacing $\delta\nu_{02}$ versus frequency for the three models with a mass of $1.497 M_{\odot}$. The continuous line corresponds to the model including rotation and atomic diffusion but no overshooting (model M1a). The dotted line denotes the model without rotation, atomic diffusion nor overshooting (model M1b), while the dashed line corresponds to a model computed without rotation or atomic diffusion, but with overshooting ($\alpha_{\text{ov}} = 0.2$). The dots indicate the observed values with an uncertainty on individual frequencies estimated to half the time resolution.

4.3 Models with a mass of $1.423 M_{\odot}$

Finally, we computed a grid of stellar models including shellular rotation and atomic diffusion with a mass of $1.423 M_{\odot}$. This mass was deduced by using only the WFPC2 measurements with the Hipparcos parallax (see Sect. 2.1). Accordingly, the observed radius of Procyon A is decreased from $2.067 \pm 0.028 R_{\odot}$ to $2.048 \pm 0.025 R_{\odot}$.

By redoing the calibration with this new mass and new observational constraint on the radius, we found the solution $t = 2.18 \pm 0.30 \text{ Gyr}$, $\alpha = 1.80 \pm 0.30$, $V_i = 17 \pm 8 \text{ km s}^{-1}$, $Y_i = 0.295 \pm 0.020$ and $(Z/X)_i = 0.0231 \pm 0.0015$. The position of this model (denoted model M3 in the following) in the HR diagram is shown in Fig. 1, while the characteristics of this model are given in Table 2. The modeling parameters of this M3 model are also very similar to the ones of the other rotating models, apart from a larger age, which results directly from the lower mass of the star.

One can see from Table 2 and Fig. 1 that the agreement between the theoretical and observed global parameters of Procyon A is somewhat better for the more massive models (models M1 and M2) than for this M3 model. This is especially true for the radius of $2.024 R_{\odot}$ which lies in the lower border of the observed box (see Fig. 1). This is due to the fact that the radius of this model has to be lower than the radii of the other models in order to compensate the mass

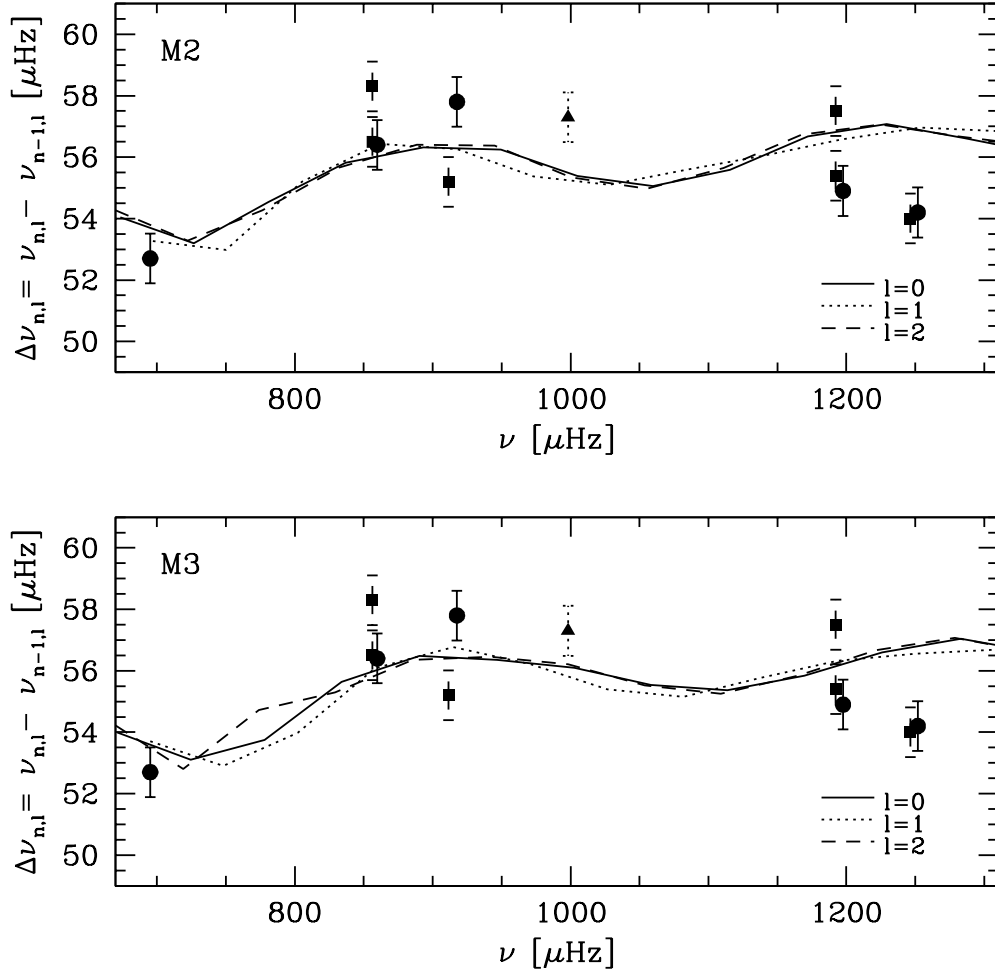


Fig. 7. Large spacing versus frequency for the models with masses of $1.465 M_{\odot}$ (model M2) and $1.423 M_{\odot}$ (model M3). Both models include the effects of rotation and atomic diffusion. The dots indicate the observed values of the large spacing with an uncertainty on individual frequencies estimated to half the time resolution.

decrease and to keep a value of the mean large spacing close to the observed value of $55.5 \mu\text{Hz}$. Besides, one can see on Fig. 2 that the theoretical large spacings of the M3 model are in good agreement with the observed ones. The echelle diagram of Fig. 8 shows that the p -modes frequencies of the M3 model are compatible with the asteroseismic observations, even if the agreement is better for the more massive M1 models than for this model.

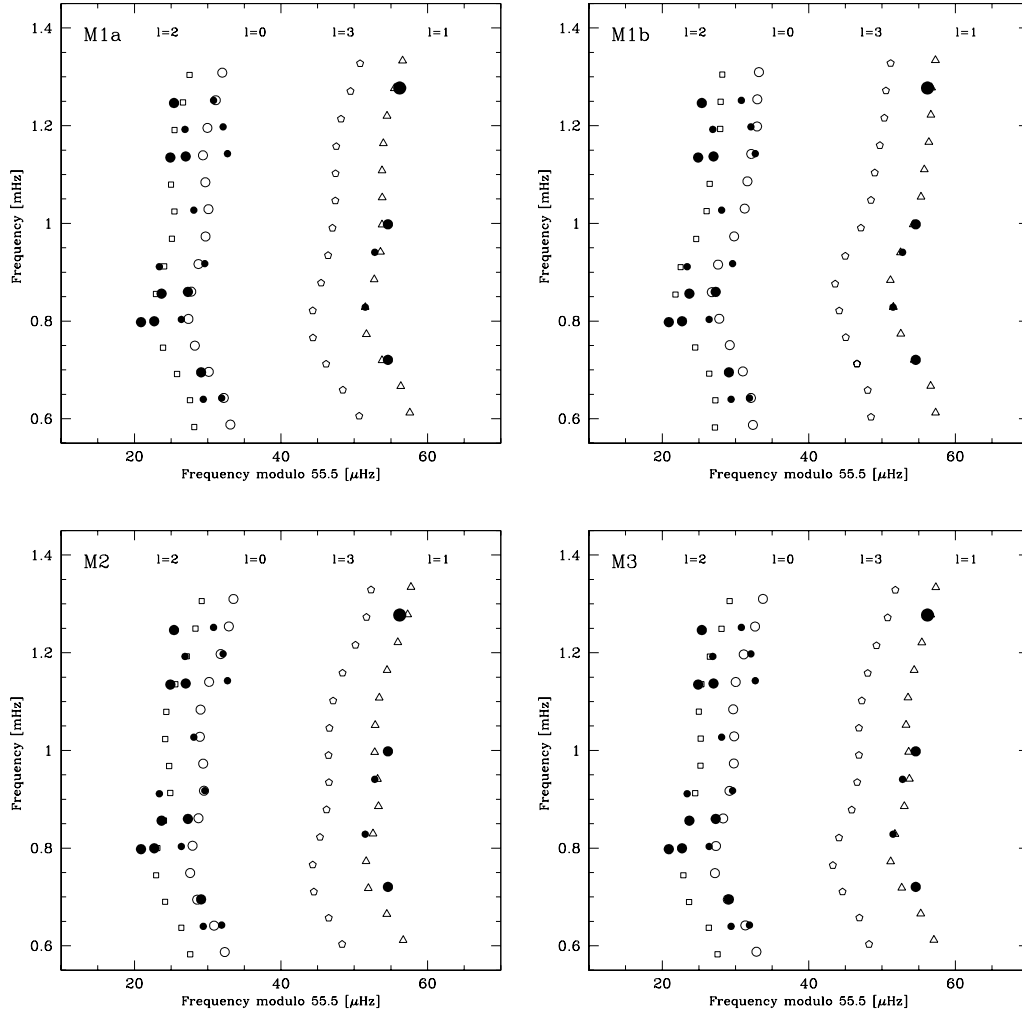


Fig. 8. Echelle diagrams for the four models of Procyon A listed in Table 2. Open symbols refer to theoretical frequencies, while the filled circles correspond to the observed frequencies (see ECBB04). Open circles are used for modes with $\ell = 0$, triangles for $\ell = 1$, squares for $\ell = 2$ and pentagons for $\ell = 3$. The models with a mass of $1.497 M_{\odot}$ are in better accordance with the asteroseismic data than the less massive M2 and M3 models.

5 Conclusion

By combining all non-asteroseismic observables with the asteroseismic measurements of ECBB04, we find that the observed mean large spacing of $55.5 \pm 0.5 \mu\text{Hz}$ favours a mass of $1.497 M_{\odot}$ for Procyon A. Indeed, the lower masses of 1.465 and $1.423 M_{\odot}$ lead to models which are in less good agreement with the observational constraints. We also determine the following global parameters of Procyon A: an age of $t = 1.72 \pm 0.30$ Gyr, an initial helium mass fraction $Y_i = 0.290 \pm 0.010$, a nearly solar initial metallicity $(Z/X)_i = 0.0234 \pm 0.0015$ and a mixing-length parameter $\alpha = 1.75 \pm 0.40$.

Note that the lower value of $53.6 \pm 0.5 \mu\text{Hz}$ reported by Martić et al. (2004) favours the lower mass of $1.423 M_{\odot}$ (Kervella et al. 2004). This can be immediately understood by recalling that the mean large spacing is proportional to the square root of the star’s mean density. Since the radius of Procyon A is now precisely determined (thanks to interferometric measurements), a lower value of the mean large spacing results in a lower value of the mass.

We also show that the effects of rotation on the inner structure of the star may be revealed by asteroseismic observations, if precise measurements of the small spacings between $\ell = 2$ and $\ell = 0$ modes can be determined. Indeed, there are subtle differences in the frequency dependence of the small spacing between rotating and non-rotating models, which results from changes in the size and in the outer border of the star’s convective core. As expected for small initial velocities, these rotational effects are found to mimic the effects due to an overshoot of the convective core into the radiative zone. Unfortunately, the asteroseismic observations now available for Procyon A are not accurate enough to enable us to discuss these subtle differences.

We conclude that the combination of all non-asteroseismic measurements with existing asteroseismic observations puts important constraints on the global parameters of Procyon A, but that more accurate asteroseismic data are needed to really test the physics of the stellar models.

Acknowledgements

We would like to thank J. Christensen-Dalsgaard for providing us with the Aarhus adiabatic pulsation code. We also thank A. Maeder, G. Meynet, C. Charbonnel and S. Talon for helpful advices. This work was partly supported by the Swiss National Science Foundation.

References

- Allende Prieto, C., Asplund, M., López, R.J.G., et al. 2002, *ApJ*, 567, 544 (2002ApJ...567..544A)
- Angulo, C., et al. 1999, *Nucl. Phys. A*, 656, 3 (1999NuPhA.656...3A)
- Barban, C., Michel, E., Martić, M., et al. 1999, *A&A*, 350, 617 (1999A&A...350..617B)
- Bouchy, F., Maeder, A., Mayor, M., et al. 2004, *Nature*, in press
- Bouvier, J., Forestini, M., & Allain, S. 1997, *A&A*, 326, 1023 (1997A&A...326.1023B)

- Brown, T.M., Gilliland, R.L., Noyes, R.W., & Ramsey, L.W. 1991, *ApJ*, 368, 599 (1991ApJ...368..599B)
- Chaboyer, B., Demarque, P., & Guenther, D.B. 1999, *ApJ*, 525, L41 (1999ApJ...525L..41C)
- Christensen-Dalsgaard, J. 1997,
<http://astro.phys.au.dk/~jcd/adipack.n/>
- Christensen-Dalsgaard, J., & Kjeldsen, H. 2004, *Nature*, 430, 29 (2004Natur.430...29C)
- Demarque, P., & Guenther, D.B. 1988, in: *Advances in Helio- and Asteroseismology*, ed. J. Christensen-Dalsgaard & S. Frandsen, *IAU Symp.*, 123, 287 (1988IAUS...123..287D)
- Di Mauro, M.P., Christensen-Dalsgaard, J. 2001, in: *Recent Insights into the Physics of the Sun and Heliosphere: Highlights from SOHO and Other Space Missions*, ed. P. Brekke, B. Fleck, & J.B. Gurman, *IAU Symp.*, 203, 94 (2001IAUS...203...94D)
- Eggenberger, P., Charbonnel, C., Talon, S., Meynet, G., Maeder, A., Carrier, F., & Bourban, G. 2004a, *A&A*, 417, 235 (2004A&A...417..235E)
- Eggenberger, P., Carrier, F., Bouchy, F., & Blecha, A. 2004b, *A&A*, 422, 247 (2004A&A...422..247E)
- Flower, P. 1996, *ApJ*, 469, 355 (1996ApJ...469..355F)
- Fuhrmann, K., Pfeiffer, M., Franck, C., et al. 1997, *A&A*, 323, 909 (1997A&A...323..909F)
- Girard, T.M., Wu, H., Lee, J.T., et al. 1996, *BAAS*, 188, 6002 (1996AAS...188.6002G)
- Girard, T.M., Wu, H., Lee, J.T., et al. 2000, *AJ*, 119, 2428 (2000AJ....119.2428G)
- Grevesse, N., & Sauval, A.J. 1998, *Space Sci. Rev.*, 85, 161 (1998SSRv...85..161G)
- Guenther, D.B., & Demarque, P. 1993, *ApJ*, 405, 298 (1993ApJ...405..298G)
- Hartmann, L., Garrison Jr., L.M., & Katz, A. 1975, *ApJ*, 199, 127 (1975ApJ...199..127H)
- Irwin, A.W., Flechter, J.M., Yang, S.L.S., & Walker, G.A.H. 1992, 104, 489 (1992PASP...104..489I)
- Kawaler, S.D. 1988, *ApJ*, 333, 236 (1988ApJ...333..236K)
- Kervella, P., Thévenin, F., Morel, P., et al. 2004, *A&A*, 413, 251 (2004A&A...413..251K)
- Lejeune, T., Cuisinier, F., & Buser, R. 1998, *A&AS*, 130, 65 (1998A&AS...130...65L)
- Maeder, A. 2003, *A&A*, 399, 263 (2003A&A...399..263M)

- Martić, M., Schmitt, J., Lebrun, J.-C., et al. 1999, *A&A*, 351, 993 (1999A&A...351..993M)
- Martić, M., Lebrun, J.-C., Appourchaux, T., & Korzennik, S.G. 2004, *A&A*, 418, 295 (2004A&A...418..295M)
- Matthews, J.M., Kusching, R., Guenther, D.B., et al. 2004, *Nature*, 430, 51 (2004Natur.430...51M)
- Meynet, G., & Maeder, A. 2000, *A&A*, 361, 101 (2000A&A...361..101M)
- Paquette, C., Pelletier, C., Fontaine, G., & Michaud, G. 1986, *ApJ*, 61, 177 (1986ApJS...61..177P)
- Provost, J., Martić, M., Berthomieu, G., & Morel, P. 2002, in: *Proceedings of the First Eddington Workshop on Stellar Structure and Habitable Planet Finding*, ESA SP-485, Noordwijk, The Netherlands, 309 (2002sshp.conf..309P)
- Richard, O., Vauclair, S., Charbonnel, C., & Dziembowski, W.A. 1996, 312, 1000 (1996A&A...312.1000R)
- Schaller, G., Schaerer, D., Meynet, G., et al. 1992, *A&AS*, 96, 269 (1992A&AS...96..269S)
- Strand, K. Aa 1951, *ApJ*, 113, 1 (1951ApJ...113....1S)